Genes & Diseases (2020) 7, 424–439

Available online at www.sciencedirect.com

ScienceDirect

journal homepage: http://ees.elsevier.com/gendis/default.asp

FULL LENGTH ARTICLE

Identification of miRNA signature associated with BMP2 and chemosensitivity of TMZ in glioblastoma stem-like cells

Xiaoyu Guo [a,1], Ziguo Luo [a,1], Tong Xia [a], Lanxiang Wu [a], Yanshu Shi [b], Ying Li [a,*]

[a] *Life Science Institute, Chongqing Medical University, Chongqing, China*
[b] *Department of Radiology, Southwest Hospital, Third Military Medical University, Chongqing, China*

Received 4 April 2019; received in revised form 12 June 2019; accepted 4 September 2019
Available online 9 September 2019

KEYWORDS
BMP2;
Cancer stem cell;
CeRNA;
Gliobalstoma;
RNA-seq;
TMZ

Abstract Glioblastoma multiform (GBM) is the most lethal intracranial tumor in adults. Glioblastoma stem-like cells (GSCs) are responsible for tumorigenesis and chemotherapy resistance. BMPs are known to increase temozolomide (TMZ) response in GSCs, however, the intracellular molecular mechanism remains largely unknown. In this study, we built a GSC cell model called U87S, and performed RNA sequencing to identify differentially expressed (DE) miRNA profiles in U87S cells treated with BMP2, TMZ or combined BMP2 and TMZ respectively. Bioinformatics analysis revealed that most DE miRNAs were involved in the cancer pathways, suggesting their crucial roles in gliomagenesis. Eight miRNAs from RNA-seq were validated. Four out of these miRNAs (*has-miR-199a-3p*, *hsa-miR-374b-5p*, *hsa-miR-320d*, and *hsa-miR-339-5p*) were found significantly up-regulated in GBM tumor tissues. One of them, *hsa-miR-199a-3p*, was significantly correlated with the survival of GBM patients, and differentially expressed in U87S cells. Expression of *hsa-miR-199a-3p* was up-regulated by BMP. Overexpression of *hsa-miR-199a-3p* in U87S cells inhibited cell viability and enhanced the cytotoxicity of TMZ. And activation of BMP boosted the effect of *hsa-miR-199a-3p* on cell viability and TMZ-mediated cytotoxicity. Besides, expressions of five predicted targets of *hsa-miR-199a-3p* were evaluated. Four of them were differentially expressed in GBM tumors. And one of them, SLC22A18, was associated with the survival of GBM patients. In the end, a *hsa-miR-199a-3p*-mediated ceRNA network was constructed for the convenience of future study. Together, our data provided DE miRNA expression profiles associated with BMP2 and TMZ in GSCs, which

* Corresponding author. Life Science Institute, Chongqing Medical University, 1 Xueyuan Road, District Yuzhong, Chongqing, 400016, China.
E-mail address: liying@cqmu.edu.cn (Y. Li).
Peer review under responsibility of Chongqing Medical University.
[1] Represents equal contribution.

https://doi.org/10.1016/j.gendis.2019.09.002

might lead to finding out miRNA-based target therapies that specially target GSCs.

Introduction

Glioblastoma multiform (GBM) is one of the most lethal malignant tumors of the central nervous system in adults, characterized by rapid diffusion, infiltrating growth and cytological heterogeneity in a huge high level.[1] Current standard treatment across the globe for GBM includes surgical resection, followed by simultaneous radiotherapy and adjuvant chemotherapy.[2] However, the median survival time with optimal treatment is only about 14 months, while the 5-year survival rate is close to or below 5%.[3] Temozolomide (TMZ) is the most commonly used alkylating agent for treating GBM. Unfortunately, GBM often exhibits resistance to TMZ, which is one of the most reasons for GBM recurrence.[2] Growing evidence have notarized the existence of a subpopulation of tumor cells with stem-like properties, known as glioblastoma stem-like cells (GSCs),[4,5] which possess ability of self-renewal, multipotential differentiation and maintained proliferation. There is compelling evidence showing that GSCs can survive the traditional radio- or chemotherapy, responsible for the tumor-progression, treatment-resistant and tumor recurrence.[6–8] Therefore, targeting GSCs would be a promising approach for treating glioblastoma. However, the underlying molecular mechanism of chemoresistance of GSCs is not completely understood.

Bone morphogenetic proteins (BMPs) are a family of evolutionarily conserved growth factors and morphogens most of which belong to the Transforming Growth Factor β (TGF-β) superfamily. Many studies have revealed that BMPs not only regulate bone and cartilage, but exert a wide variety of biological processes in development and cancers.[9] To date, more than 20 kinds of BMP ligands have been identified in humans. Based on the homology of amino acid sequences, BMPs are classified into three groups. The first subgroup contains BMP-2 and BMP-4; the second group is consisted of BMP- 5, BMP-6, BMP-7 and BMP-8; while BMP-9 and BMP-10 comprise the third osteogenic group.[10] The rough backbone of the canonical BMP signaling pathways has been well illustrated.[11,12] Briefly, BMP ligands bind to membranal serin-threonine kinase receptors (type I and type II) to form a heterotetrameric complex, which then binds to and phosphorylates the receptor-activated SMADs (R-SMADs). Next, activated R-SMADs bind to the common SMAD (Co-SMAD) to form a complex, which then translocates to the nucleus to drive the target genes expression together with other transcription factors.[13] BMP signaling is tightly regulated at different levels, by both extracellular antagonists and intracellular modulators such as the inhibitory SMAD (I-SMAD), which acts in a negative feedback loop in response to active BMP signaling. It has been well known that BMPs play important roles in GBM progress and clearly linked to tumor malignancy.[14] Expression of the BMP type IB receptor and the ligand BMP2 are both higher expressed in GBM than in low-grade gliomas.[15,16] The expression level of BMP2 is also related to tumor malignancy and GBM patient survival, therefore being considered as a prognostic marker for human glioma.[17,18] In addition, BMP4 and analogously BMP2 treatments have been found to reduce GSC cell proliferation and be strong inducers of astroglial differentiation in GSC cells both *in vitro* and *in vivo*.[19,20] BMP2 has also been reported to render GSCs more susceptible to TMZ treatment through destabilization of HIF-1.[17,21] Differentiation-inducing properties of BMPs make them promising candidates for GSC-targeting GBM therapy. However, GSCs have evolved mechanisms to evade BMP induced differentiation by expressing the extracellular antagonist Gremlin 1 (GREM1).[22] Further investigation of intracellular molecular mechanisms should improve outcomes towards BMP induced differentiation therapy.

microRNAs (miRNAs) are highly conserved, small non-coding RNAs with 18—25 nucleotides in length found in most eukaryotes. Typically, miRNAs function as critical regulators of posttranscriptional gene expression by binding to the 3′-untranslated region (3′-UTR) of specific mRNAs, leading to translational repression or mRNA degradation.[23] It's well known that miRNAs play widespread and critical roles in a variety of cellular processes including proliferation, differentiation, apoptosis, development, and tumor progression by regulating the expression of up to 70% of human genes.[24] Many miRNAs have been identified functionally deregulated in GBM.[25] For example, miR-21, a well studied miRNA, which is significantly highly expressed in GBM, contributes to the malignant phenotype and chemo- and radiotherapy by acting as an "oncomirs".[26] Distinct patterns of miRNA expression have been also observed in GBM compared with gliomas of lower grades,[27] so are in glioblastoma stem-like cells,[28,29] revealing their great potential to be biomarkers and therapeutic targets for GBM. However, miRNA profile is still far more being well-defined. Extensive investigation of miRNA signature in GSCs related to GBM microenvironment signals could be critical to discover an efficient therapeutic strategy.

The overall aim of this study is to identify miRNA signature which plays critical roles in the process of BMP2 effecting the chemosensitivity of TMZ in U87S cells. We built a GSC cell model called U87S, in which IC50 of TMZ was assessed and BMP signaling was confirmed to be active. Further BMP2 was demonstrated to sensitize U87S to TMZ. Next, we performed RNA sequencing with U87S cells treated with BMP2, TMZ or combined BMP2 and TMZ respectively. Differential expression profile of miRNAs was identified. Bioinformatics analysis was conducted to reveal the important roles of these DE miRNAs in gliomagenesis. Eight miRNAs were validated by RT-PCR. GO and KEGG analysis revealed that the putative targets of these eight

miRNAs were enriched in biologic regulation and PI3K-Akt pathway. One of these miRNAs, *hsa-miR-199a-3p*, was found differentially expressed in mesenchymal (M) subtype of GBM and was associated with survival outcome of patients. GO and KEGG analysis revealed that targets of *hsa-miR-199a-3p* were primarily enriched in biologic regulation and Rap1 pathway. Further, we evaluated the *hsa-miR-199a-3p* expression in cells with different differentiated levels, and found that it's differentially expressed in U87S cells. Function study showed that *hsa-miR-199a-3p* can inhibit U87S cell viability and enhance TMZ-mediated cell death. And the BMP activation can boost the functions of *hsa-miR-199a-3p* on cell viability and TMZ-induced cell death. Furthermore, Five targets of *hsa-miR-199a-3p* were validated by RT-PCR. One of them, SLC22A18, was highly expressed in GBM tumors by TCGA data, and associated with the survival outcome of patients. Furthermore, a *hsa-miR-199a-3p*-mediated ceRNA network was constructed. Together, our data may lead to finding out miRNA-based target therapies that specially target GSCs and improve outcomes towards BMP induced differentiation therapy for GBM.

Materials and methods

Cell culture and treatment

Glioblastoma cell line U87MG and astrocyte cell line HA were obtained from the Institute of Basic Medical Sciences, Chinese Academy of Medical Sciences (Beijing, China) and cultured in DMEM (Gibico, USA) supplemented with 10% fetal bovine serum (FBS) (Evergreen, China), 100 U/ml penicillin, and 100ug/ml streptomycin (Beyotime Shanghai). Glioblastoma stem-like cell line, U87S, was cultured in F-12/DMEM (Gibico, USA) with 20 ng/ml epidermal growth factor (EGF) (Gibico, USA), 20 ng/ml basic fibroblast growth factor (bFGF) (Gibico, USA), and 2% B-27 Supplement (50X) (Gibico, USA) at 37 °C in 5% CO_2.

U87S cells were harvested and dissociated. Cells were divided into four groups for RNA-seq, and treated with (1) DMSO (U87S-Cont), (2) 500 μM TMZ (U87S-TMZ) (3) 20 ng/ml BMP2 (U87S-BMP2) and (4) combined 20 ng/ml BMP2 with 500 μM TMZ (U87S-BMP2-TMZ) respectively for 24 h. TMZ (Sigma, USA) was dissolved in DMSO to create a 100 mM stock solution and stored at −20 °C before using. The final concentration of DMSO was 0.5% in both the control and the treated groups and did not exert any detectable effect on cell growth or cell death. BMP2 (Invitrogen, USA) was dissolved in aqua sterilisata. LDN 193189 (Sigma, USA), the BMP type I receptor inhibitor, was dissolved in aqua sterilisata. 200 nM LDN 193189 was used to inhibit the BMP signaling in U87S cells.

Flow cytometry and immunocytochemistry

U87S cells were harvested and dissociated into single cell suspension, then stained with PE-CD133 (Affymetrix Inc, USA) at 37 °C for 30 min. FACSVantage flow cytometer (BD Biosciences, USA) was used to monitor the percentage of CD133+ cells. For immunocytochemistry, cells were fixed with 4% paraformaldehyde for 15 min at room temperature. After the wash with PBT (0.1% Triton X-100 in 1X PBS), cells were treated with PBT containing 10% goat serum for 30 min at room temperature. The primary antibodies used were mouse-anti-CD133 (diluted 1:150, BOSTER, China), mouse-anti-GFAP (diluted 1:100, Absin, China) mouse-anti-tubulin 3 (diluted 1:200, Proteintech, China). Secondary antibodies were conjugated to dylight 488 (diluted 1:200, BOSTER, China). All primary antibodies were diluted in PBT and incubated with cells at 4 °C overnight. Secondary antibodies were typically incubated with cells for 2 h at room temperature.

Cell viability assay

Cells were seeded at 2—5 × 10^4 cells per well in a 96 multiwell plate. For detecting the IC50 of TMZ in U87S, a series of increased concentration of TMZ (0, 100, 200, 400, 600, 800, 1000, 2000 and 4000 μM) with or without BMP2 (20 ng/ml) were added to 100 ul U87S cell suspension for 24 h. And then 10ul Cell Counting Kit-8 (CCK-8, Kumamoto, Japan) was added in each well. After incubation in the dark for 3 h at 37 °C in 5% CO_2, the absorbance at 450 nm was measured by fluorescence spectrofluorometer (F-7000; Hitachi HighTechnologies Corp, Tokyo, Japan). The IC_{50} value was calculated using SPSS 20.0 software (IBM, Armonk, NY, USA). For detecting effects of *hsa-miR-199a-3p* on U87S cell viability, cells were first transfected with RNA oligos (1 pmol) for 36 h, then treated with 500 μM TMZ with or without BMP2(20 ng/ml)/LDN193189 (200 nM) for additional 24 h followed by the subsequent CCK-8 assay.

RNA isolation and RNA-seq analysis

Total RNA was isolated for four groups (U87S-Cont, U87S-TMZ, U87S-BMP2, and U87S-BMP2-TMZ). Three duplicates were for each treated group. Total RNA was extracted using Trizol Reagent (Invitrogen/Thermo Fisher Scientific, USA) according to the manufacturer's protocol. PAGE electrophoresis gel was utilized to separate the 18—30 nt RNA from total RNA. Single-strand DNA connectors, which were 5-adenylated and 3-blocked, were connected to the 3 'end of middle RNA. RT primers were added to the system to hybridize with the 3′ connector attached to the RNA and the excess free 3′ connector. To the 5′ end of the product, a primer was added for reverse transcription extension to synthesize a strand of cDNA. Then high-sensitivity polymerase was utilized to amplify cDNA and enrich cDNA with 3′ and 5′ junctions at the same time to enlarge the library yield. PAGE electrophoresis was utilized to separate PCR products in the range of 100—120 bp and removed primers, dimmers, and other by-products. Then conducted quantitative pooling and ring is pooling for the library. RNA-seq library preparation and sequencing were performed by BGI-tech (Beijing, China) using BGISE-500 for miRNA.[30,31]

The expression of genes was calculated by TPM (TPM = C*106/N)[32] for miRNA. MA-plot[33] was used to calculate the differentially expressed miRNA in three treated groups compared with U87S-cont. An absolute value of $\log_2$ (treatment/control) greater than 1 and Q value (adjust p-value) less than 0.001 was considered to be differentially expressed. Then RNAhybrid,[34] miRanda[35] and TargetScan[36] were used to predict the target genes of miRNAs.

qRT-PCR

To detect expression levels of miRNAs, total small RNAs were extracted using the miRcute miRNA isolation kit (Tiangen, China) according to the manufacturer's instruction. The reverse-transcribed complementary DNA was synthesized with miRcute Plus miRNA First-Stand cDNA Synthesis kit (Tiangen, China). Quantitative real-time polymerase chain reactions (qRT-PCR) were performed with miRcute Plus miRNA qPCR Detection Kit (SYBR Green) (Tiangen, China). RT-PCR was performed with the CFX96 touch deep well real-time PCR detection system (Bio-Rad, Hercules, California, USA). The PCR conditions started at an initial denaturation cycle (15 min at 95 °C) followed by 44 cycles of denaturation (20 s at 94 °C) and annealing/elongation (34 s at 65 °C). A melting curve analysis was conducted for each RT-PCR. The expression levels of miRNA were normalized to the internal control U6. The data were analyzed by the 2 ($^{-\triangle\triangle Ct}$) method. All experiments were performed in triplicate. The primers used for miRNA detection are listed in Table S1.

For detecting expression levels of protein-coding genes, total RNA was extracted using Trizol according to the manufacturer's protocol. The cDNA of mRNA was reverse transcribed with the Primer Script 1st Strand cDNA Synthesis Kit (TaKaRa, Japan) according to the manufacturer's instructions. And qRT-PCR amplification was performed with the SYBR green method (Takara, Japan). RT-PCR was performed with the CFX96 touch deep well real-time PCR detection system (Bio-Rad, Hercules, California, USA). The PCR conditions started at an initial denaturation cycle (30 s at 95 °C) followed by 39 cycles of denaturation (5 s at 95 °C), annealing (30 s at 65 °C), and elongation (60 s at 72 °C). A melting curve analysis was conducted for each RT-PCR. The expression levels of mRNA were normalized to the internal control GAPDH (glyceraldehyde 3-phosphate dehydrogenase). The data were analyzed by the 2 ($^{-\triangle\triangle Ct}$) method. All experiments were performed in triplicate. The primers used for miRNA detection are listed in Table S1.

Transfection of miRNAs

The *hsa-miR-199a-3p* mimics, *hsa-miR-199a-3p* inhibitor and their corresponding negative control (miR-NC and anti-NC) were the FAM modified 2-OMe-oligonucleotides, synthesized and purified using high-performance liquid chromatography at GenePharma (Shanghai, China). The sequences of the oligo sets are listed in Table S2. Cells were plated in the 96-well plate and transfected with 1 pmol oligos per well with lipofectamine RNAimax (Invitrogen Life Technologies, USA) according to the manufacturer's instructions. At 36 h post-transfection, the cells were harvested for cell viability assays.

Differential expression gene query and survival analysis

The Glioblastoma Bio Discovery Portal (GBM-BioDP)[37] is a free web-accessible resource (https://gbm-biodp.nci.nih.gov/) for accessing and displaying miRNAs differentially expressed within the subtypes of glioblastoma multiform (GBM) and potentially associated with clinical outcome of The Cancer Genome Atlas (TCGA) data.

UALCAN (http://ualcan.path.uab.edu/)[38] is an interactive web-portal for performing in-depth analyses of TCGA gene expression data. We used it to analyze the relative expression of five target genes of *hsa-miR-199a-3p* (CITED2, ANGPTL2, AGAP3, SLC22A18, and TXNIP) across 156 tumors and 5 normal samples, and to estimate the relationship between gene expression level and patient survival ratio.

Expression microarray data of GBM patient tumor samples and healthy brain tissues in GSE90603 were downloaded from the GEO dataset. Then miRNA expression pattern was analyzed by GEO2R. miRNAs were thought to be differentially expressed when the absolute value of $\log_2$ (tumor/normal) greater than 1 and adjusted $p < 0.05$.

GO and KEGG analysis

To perform Gene ontology (GO) analysis, all genes were first mapped to GO-terms in the database (http://www.geneontology.org/), which calculates the gene numbers for every term. The hyper geometric test was then used to find significantly enriched GO-terms in the input gene list. This test was based on GO: TermFinder (http://www.yeastgenome.org/help/analyze/go-term-finder). The P-value is corrected by using the Bonferroni method, a corrected P-value ≤ 0.05 is taken as a threshold. GO terms fulfilling this condition were defined as significantly enriched GO terms.

Kyoto Encyclopedia of Genes and Genomes (KEGG) pathway analysis was used to perform pathway enrichment analysis. This analysis identified significantly enriched metabolic pathways or signal transduction pathways in differential expression target genes when compared with the whole genome background.[39]

CeRNA network construction

The miRanda and TargetScan were used to identify ceRNAs (including protein-coding messenger RNAs and long non-coding RNAs), containing microRNA response elements (MREs). Then, ceRNAs which were significantly differentially expressed in our RNA-seq data were selected to predict the global interactions with *hsa-miR-199a-3p*.

Statistic analysis

SPSS version 17.0 software was used to carry out all statistical analyses. Data were presented as means ± SD ($n \geq 3$). Differences between the means of the treatment and control groups were analyzed using a two-tailed Student's t-test. P value ≤ 0.05 was considered statistically significant.

Results

Identification of U87S GSCs derived from U87MG

To get glioblastoma stem-like cells, we enriched GSCs from human glioblastoma U87MG cells culturing in the serum-

free neurosphere culture medium. After 10—14 days, spheres were formed, at a size of approximately 50—100 μM (Fig. 1A), showing the ability of self-renewal. Immunostaining revealed that these spheres were positive for stemness marker CD133 (Prominin-1) (Fig. 1A). Flow cytometry analysis showed the percentage of CD133+ positive cells in U87S spheres was up to 89.34% compared to 1.28% in U87MG (Fig. 1B). CD133+ cells were further sorted through fluorescence activated cell sorting, and then named as U87S. To examine the multipotential differentiation capacity of U87S cells, U87S cells were dissociated and seeded into the differentiation medium containing 2% FBS for 10 days. More than 90.0% cells were flat with short processes, positively immunostained for the astroglial marker, GFAP (Glial fibrillary acidic protein), and fewer cells, about 3.0%, were flat with elongated bipolar or tripolar processes, positively immunostained for the neuronal marker, β tubulin-III (Fig. 1C). Our results demonstrated that U87S cells have multidirectional differentiation capacity.

BMP sensitizes U87S cells to temozolomide

To use U87S as a model to screen miRNAs associated with BMP signaling and related to the chemotherapeutic agent TMZ, first, we tested the effect of TMZ on U87S cells. For calculating IC50 of TMZ, cells were treated with a gradient concentration of TMZ. Cell viability was monitored by CCK-8 assay. We observed that TMZ-induced U87S cell death in a dose-dependent manner (Fig. 2A). Based on the data of the cell viability, IC50 of TMZ in U87S was 725 μM (Fig. 2A), significantly higher than the ones in U87 MG (glioblastoma cells, 479 μM) and HA (astrocytes, 275 μM). Our results demonstrated that glioblastoma stem-like cells are more

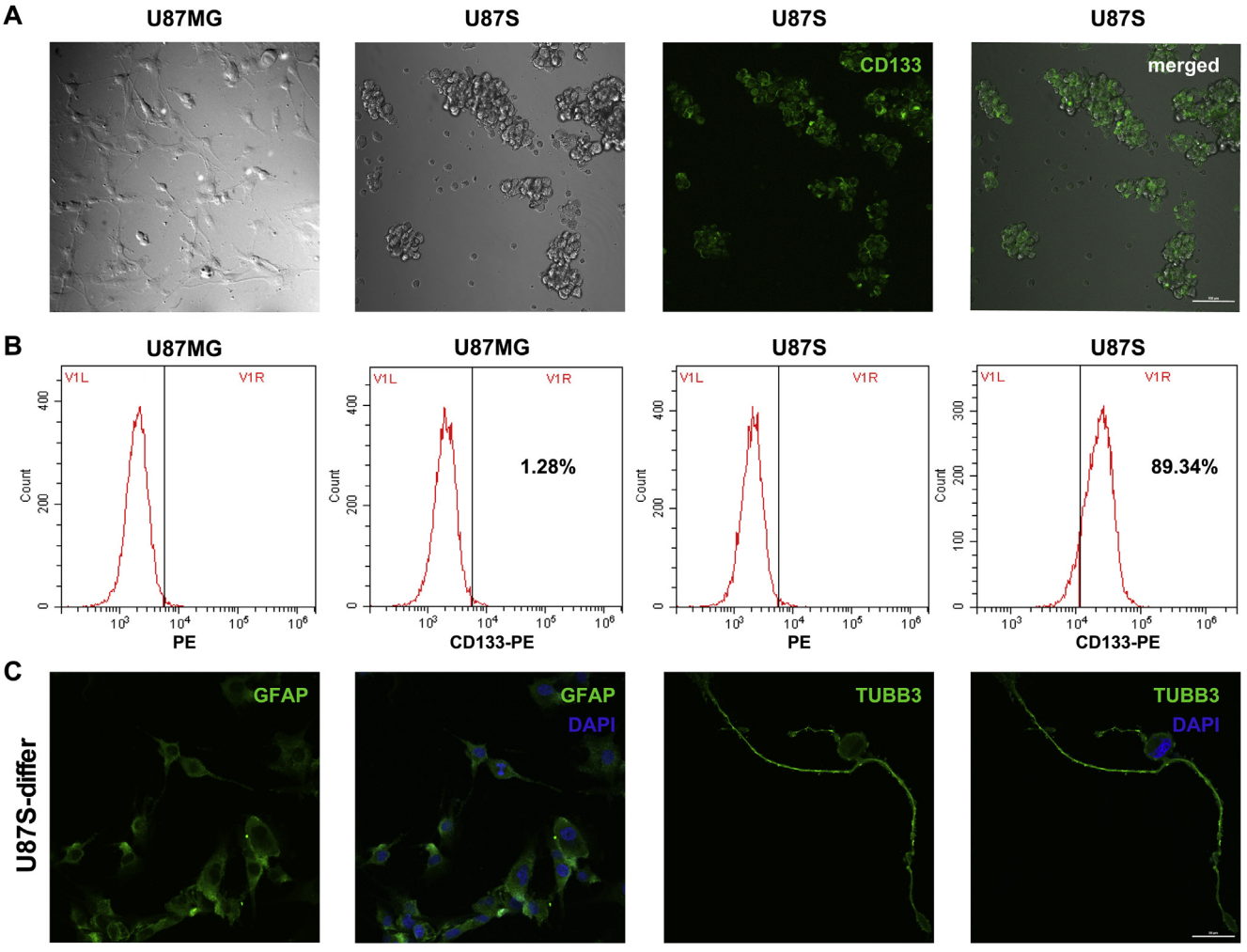

Figure 1 Characterization of U87S GSCs derived from U87MG. (**A**) Morphologies of U87MG vs. U87S cells. Most of the adherent growth U87MG cells are showing astrocyte-like morphology, flat cell body with short processes. The U87S cells are cultured in the serum-free neurosphere culture medium. Spheres are at the size of approximately 50—100 μM, showing positive immunofluorescence staining of stemness marker CD133 (Prominin-1) (green). (**B**) Flow cytometry analysis shows the percentage of CD133+ positive cells in U87S spheres was up to 89.34%, compared to 1.28% in U87MG. (**C**) U87S cells possess a multipotential differentiation capacity. U87S cells were dissociated and seeded into the differentiation medium containing 2% FBS for 10 days. Representative immunofluorescence staining for the astroglial marker, GFAP, and the neuronal marker, β tubulin-III (TUBB3) respectively. Scale bar in A is 100 μM, scale bare in C is 50 μM.

resistant to TMZ compared to GBM cells and normal astrocytes, consistent with others' reports.[40,41] Furthermore, we studied the effect of BMP signaling on the chemosensitivity of U87S to TMZ. BMP2 (20 ng/ml) was utilized to activate BMP signaling and LDN 193189 (200 nM), the BMP type I receptor inhibitor,[42] was used to inhibit endogenous BMP signaling, respectively. The expression levels of intracellular BMP signaling effectors, SMAD1 and SMAD5, and transcriptional targets of BMP signaling, SMAD6 and ID1 (inhibitor of DNA binding 1), were examined to confirm the change of BMP signaling. Addition of recombinant 20 ng/ml BMP2 (0 μM TMZ) or 200 nM LDN 193189 (0 μM TMZ) caused significant change on the expression levels of these intracellular BMP signaling effectors (Fig. 2C, fold change >2 compared to untreated control, $p < 0.05$), but did not show marked change on U87S cell viability (Fig. 2B, 0 μM TMZ). However, when U87S cells were exposed to TMZ, co-treatment of BMP2 markedly reduced the cell viability, while co-treatment of LDN 193189 significantly increased the cell viability (Fig. 2B, $p < 0.05$). Our result demonstrated that the activation of BMP signaling can sensitize U87S cells to TMZ, suggesting that U87S is an ideal GSC cell model for screening intracellular miRNA signatures associated with BMP and TMZ.

Differentially expressed miRNAs and functional analysis

In order to identify miRNA profiles associated with BMP and TMZ in GSC cells, we treated U87S cells with BMP2 (20 ng/ml), TMZ (500 μM), or combination of BMP2 and TMZ respectively, and performed transcriptome sequencing to profile differentially expressed (DE) miRNA in these three treated groups (U87S-BMP2, U87S-TMZ, and U87S-BMP2-TMZ). We selected significant DE miRNAs with a log2 (ratio) of more than or equal to 1.0 or less than or equal to −0.5, and a Q (adjusted p-value) < 0.001. In total, there were 184 miRNAs (106 up-regulated, 78 down-regulated) significantly deregulated in U87S-TMZ compared with untreated U87S (Table S3), 95 differentially expressed miRNAs (58 up-regulated, 37 down-regulated) in U87S-BMP2 compared with U87S (Table S4), and 162 miRNAs (83 up-regulated, 79 down-regulated) significantly expressed in U87S-BMP2-TMZ compared with U87S (Table S5). Hierarchical clustering showed that most of these DE miRNAs had similar expression patterns in three treated groups (Fig. 3A). Among these DE miRNAs, 94 miRNAs were differentially expressed both in U87S-TMZ and U87S-BMP2-TMZ, 69 miRNAs were differentially expressed both in U87S-BMP2 and U87S-BMP2-TMZ, and 39 miRNAs were differentially expressed in all three treated groups (Fig. 3B).

Further, to understand the potential functions of these DE miRNAs, we predicted the target genes for these DE miRNAs with three commonly used algorithms, TargetScan, miRanda, and RNAhybrid. In total, 48957 putative mRNA targets for 184 DE miRNAs in U87S-TMZ, 39850 mRNAs for 95 DE miRNAs in U87S-BMP2 and 48038 mRNAs for 162 DE miRNAs in U87S-BMP2-TMZ were detected. Gene Ontology

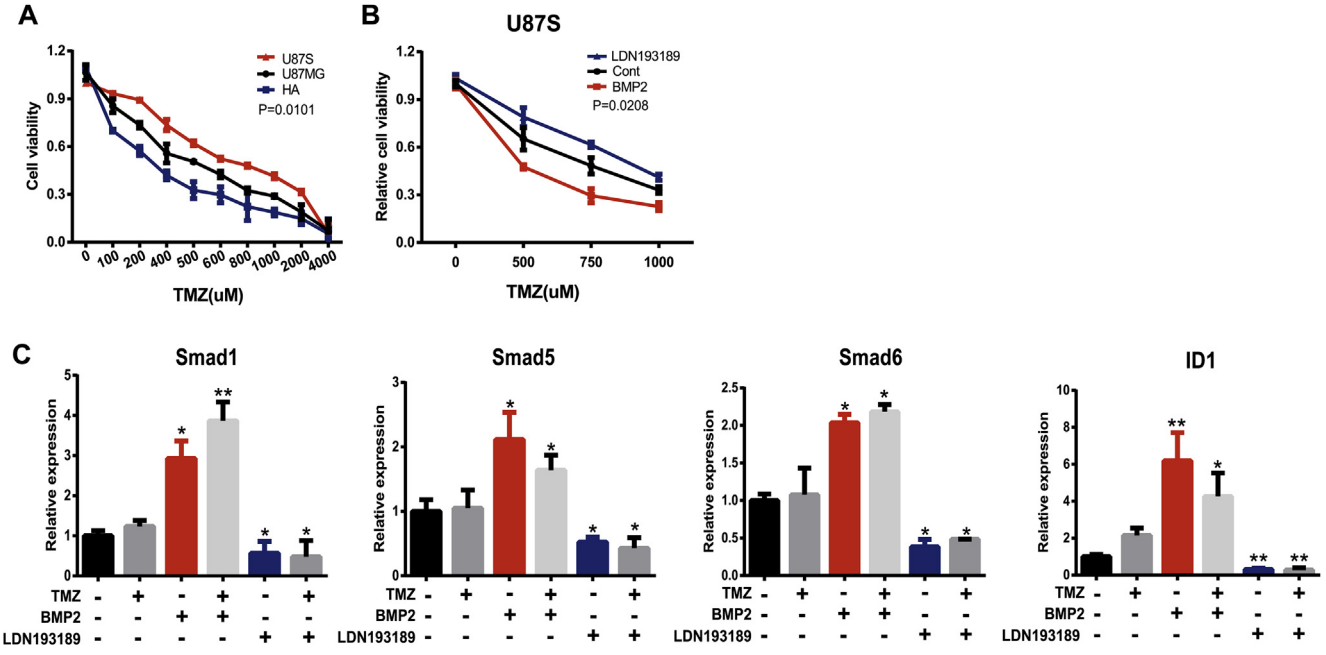

Figure 2 BMP2 sensitizes U87S cells to temozolomide. (**A**) Cytotoxic effect of TMZ on U87S cells. U87S cells were treated with TMZ at assigned concentrations (0—4000 μM) for 24 h. Cell viability was measured by CCK-8 assay. IC50 of TMZ is 725 μM, 479 μM, and 275 μM in U87S, U87MG, and HA. The data are given as the means ± SD of three replicates. (**B**) BMP2 sensitizes U87S cells to TMZ. U87S cells were treated with a series of TMZ (0—1000 μM) alone (black curve), together with 20 ng/ml recombinant BMP2 (red curve) or 200 nM LDN 193189. Cell viability was measured by CCK-8 assay. The data are given as the means ± SD of three replicates. (**C**) BMP signaling pathway is active in U87S cells. mRNA expression levels of intracellular BMP signaling effectors, SMAD1 and SMAD5, and transcriptional targets of BMP signaling, SMAD6, and ID1 by qRT-PCR. Data is normalized vs. endogenous control: GAPDH. Results are shown in relative expression and data are means ± SD from three independent experiments. *$p < 0.05$, and **$p < 0.01$.

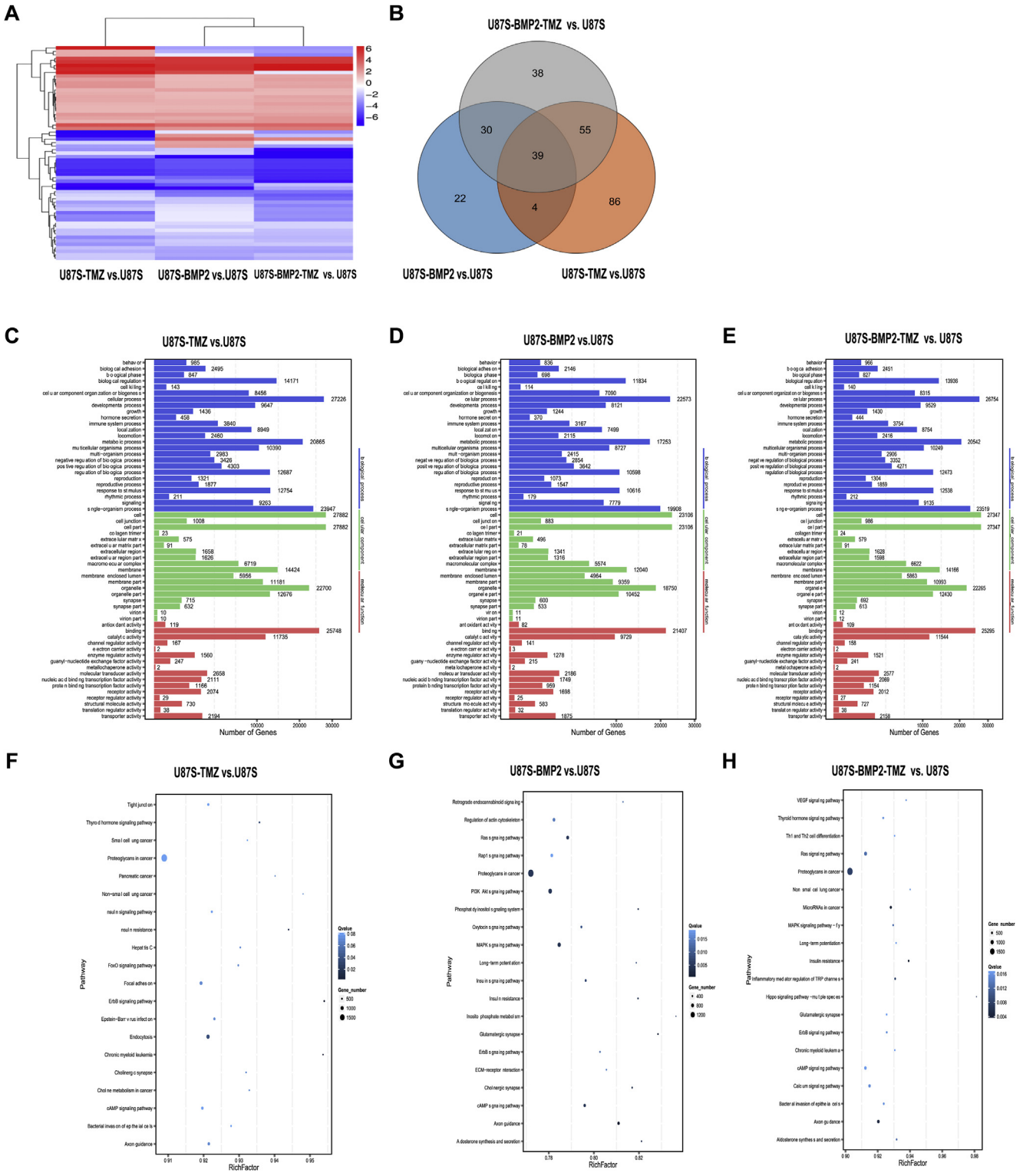

Figure 3 Differentially expressed miRNAs by RNA-seq. (**A**) Heatmap of hierarchical clustering analysis of differentially expressed miRNAs in three treated groups (U87S-BMP, U87S-TMZ, and U87S-BMP-TMZ), (fold change $>$ 2, compared to untreated U87S respectively, FDR (false-discovery rate) $<$ 0.001). Red color represents up-regulated miRNAs and blue color represents down-regulated miRNAs. Expression data are represented as log2 fold change versus U87S for each group. (B) Venn diagram reports the differentially expressed miRNAs in three treated groups, U87S-BMP, U87S-TMZ, and U87S-BMP-TMZ. (**C-E**) Functional enrichment analysis of putative target genes of DE miRNAs by GO. The ar chart represents the classification of GO Biological Processes, Cellular Component or Molecular Function. Bars represent the number of genes in the specified category, organized by p-value. (**F**—**H**) The top 20 enriched signaling pathways for putative target genes of DE miRNAs by KEGG. Enriched pathways are selected based on the enrichment factor value with the number of genes in a pathway $\geq$4. The blue color from dark to light represents the Q value. The size of the dots represents the gene number in each pathway.

(GO) and KEGG analysis were performed to identify biological processes and pathways associated with these target genes (Fig. 3C—H). All three treated groups showed similar patterns for GO classification (Fig. 3C—E). Target mRNAs of DE miRNAs were mainly involved in the biological processes, such as cellular process, metabolic process, biological regulation, response to stimulus, and regulation of biological process. The molecular function of these target mRNAs was mainly related to binding. And KEGG enrichment pathway analysis (Fig. 3F—H) revealed that, most target mRNAs of DE miRNAs in all three treated groups were enriched in proteoglycans in the cancer signaling pathway. In addition, target genes of DE miRNAs in the BMP2-treated group were also enriched in glioma-related pathways, such as P13K-Akt (phosphatidylinositol-3 kinases/the protein kinase B) signaling pathway, MAPK (Mitogen-Activated Protein Kinase) signaling pathway and Rap1 signaling pathway. Together, our data indicate that miRNAs may play critical roles in the process of BMP2-mediated TMZ sensitivity in U87S.

Validation of differentially expressed miRNAs

To confirm the miRNA-sequencing results, we used qRT-PCR to assess the expression of eight miRNAs at transcriptional level (Table 1 and Fig. 4A). Two DE miRNAs (*hsa-miR-199a-3p* and *hsa-miR-33a-5p*) were up-regulated both in U87S-BMP2 and U87S-BMP2-TMZ, but not in U87S-TMZ, representing miRNAs under regulation of BMP2, but not changed by TMZ. Two miRNAs (up-regulated *hsa-miR-409-3p* and down-regulated *hsa-miR-374b-5p*) were differentially expressed both in U87S-TMZ and U87S-BMP2-TMZ, but not in U87S-BMP2, representing miRNAs deregulated by TMZ, but not by BMP2. Three DE miRNAs (up-regulated *hsa-miR-27a-5p* and *hsa-miR-376b-5p*, down-regulated *has-miR-320d*) were deregulated in U87S-BMP2, U87S-TMZ, and U87S-BMP2-TMZ, representing miRNAs regulated by both BMP2 and TMZ. *hsa-miR-339-5p* was up-regulated in U87S-TMZ, but down-regulated in U87S-BMP2 and U87S-BMP2-TMZ, indicating that BMP2 can counteract TMZ's effect on the expression of *hsa-miR-339-5p*. Our qRT-PCR results were consistent with the sequencing data, suggesting that miRNA signatures identified by our miRNA sequencing are reliable.

Further, to understand the potential functions of these eight validated miRNAs, we predicted the target genes for these eight miRNAs. In total, 7379 mRNAs were predicted to be targets of these eight miRNAs. Gene Ontology (GO) analysis was performed to identify biological processes associated with the miRNA target genes. The primarily enriched biological processes included cellular process, metabolic process, biological regulation and response to stimulus. The most enriched molecular functions of these target genes included binding, catalytic activity and molecular transducer activity (Fig. 4B). KEGG pathway analysis revealed that most of these miRNA targets were enriched in the PI3K-Akt signaling pathway (Fig. 4C), a well-known glioma-related pathway, suggesting the important roles of these eight miRNAs in gliomagenesis.

hsa-miR-199a-3p is associated with the survival of GBM patients

To explore the importance of these 8 validated miRNAs in GBM, we analyzed their expression levels between 7 wild-type brain tissues and 16 GBM tumor tissues in GSE datasets (GSE90603). 4 out of 8 miRNAs (*has-miR-199a-3p*, *hsa-miR-374b-5p*, *hsa-miR-320d*, and *hsa-miR-339-5p*) were found markedly up-regulated in GBM tumor tissues (fold change ≥ 2, $p < 0.05$) (Fig. 5A).

GBM can be divided into different subtypes, including classical (C), mesenchymal (M), proneural (P), and neural (N) according to the transcriptomic classification.[43] miRNAs have been known to be differentially expressed in different subtypes of glioblastoma, and associated with survival of GBM patients.[44,45] To further explore the potential importance of 8 validated miRNAs in GBM, we queried the miRNAs expression in subtypes of GBM from TCGA dataset with GBM-BioDP,[37] and got results for two validated miRNAs, *hsa-miR-199a-3p* and *hsa-miR-409-3p*. These two miRNAs had different expression patterns between subtypes of GBM in 196 TCGA patients (Fig. 5B and C). *hsa-miR-199a-3p* showed significantly elevated expression in M subtype of GBM patients ($p = 0.001$), while *hsa-miR-409-3p* did not show a significant difference of expression between GBM subtypes. When the expression level of a single miRNA was considered, Kaplan-Meier survival rate analysis confirmed that higher expression of *hsa-miR-199a-3p* in C ($p = 0.02$) and M subtypes ($p = 0.029$) was associated with better survival outcome (Fig. 5D). The expression level of *hsa-miR-199a-3p* in P subtype patients did not show a significant effect on

Table 1 List of Differentially expressed miRNAs by RNA-seq.

miRNA	U87S-BMP2 Log_2 (FC)	*p*- Value	U87S-TMZ Log_2 (FC)	*p*- Value	U87S-BMP2-TMZ Log_2 (FC)	*p*- Value
hsa-miR-199a-3p	3.396	0.00000	0.387	0.20300	2.680	0.00000
hsa-miR-33a-5p	1.834	0.00000	0.738	0.09036	2.598	0.00000
hsa-miR-409-3p	0.767	0.56000	1.797	0.00000	1.797	0.00000
hsa-miR-374b-5p	−0.673	0.49800	−1.820	0.00000	−3.897	0.00000
hsa-miR-27b-5p	3.131	0.00000	3.871	0.00000	3.172	0.00000
hsa-miR-376b-5p	1.747	0.00000	1.185	0.00002	1.952	0.00000
hsa-miR-320d	−1.881	0.00000	−1.351	0.00000	−4.016	0.00000
hsa-miR-339-5p	−2.321	0.00000	1.298	0.00000	−2.842	0.00000

FC: fold change. Positive and negative values for Log_2(FC) represent miRNAs up-regulated or down-regulated, respectively, upon treatment of BMP2, TMZ or combined BMP2 and TMZ.

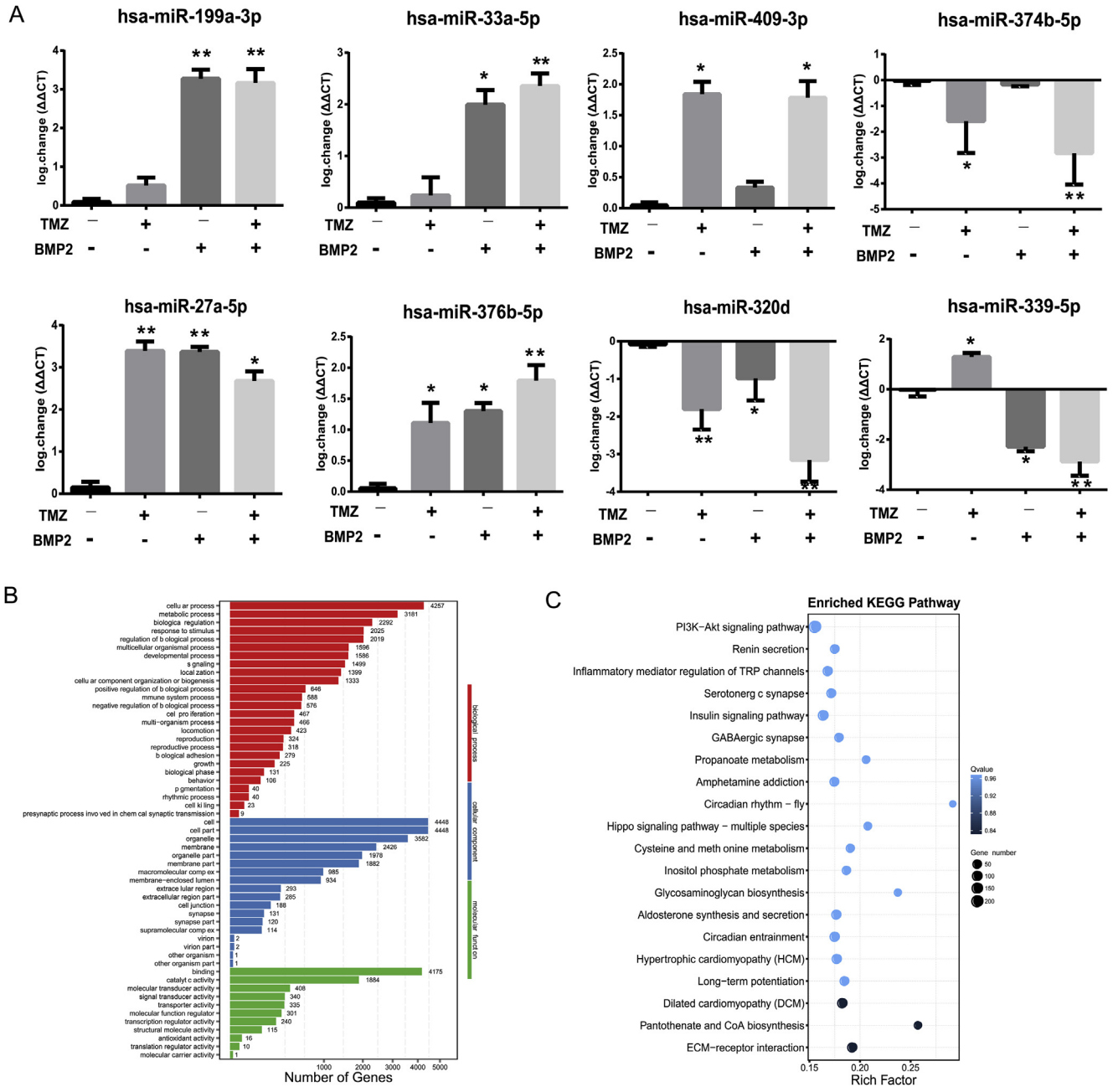

Figure 4 Validation of 8 differentially expressed miRNAs and GO and KEGG analysis. (**A**) qRT-PCR was performed to assess relative miRNA expression of *hsa-miR-199a-3p*, *hsa-miR-33a-5p*, *hsa-miR-409-3p*, *hsa-miR-374b-5p*, *hsa-miR-27a-5p*, *hsa-miR-376b-5p*, and *has-miR-320d*. Data are presented as mean ± SD from three independent experiments. *$p < 0.05$ compared with untreated group, and **$p < 0.01$ compared with the untreated group. (**B**) Functional enrichment analysis of putative 7379 targets genes of 8 validated miRNAs by GO. The bar chart represents the classification of GO Biological Processes, Cellular Component or Molecular Function. Bars represent the number of genes in the specified category, organized by p-value. (**C**) The top 20 enriched signaling pathways for putative target genes of 8 validated miRNAs by KEGG. Enriched pathways are selected based on the enrichment factor value with the number of genes in a pathway ≥4. The blue color from dark to light represents the Q value. The size of the dots represents the gene number in each pathway.

the survival time. While the expression level of another miRNA, *hsa-miR-409-3p* in each GBM subtype was not significantly associated with the survival time of patients (Fig. 5E). However, interestingly, when the expression levels of *hsa-miR-409-3p* and *hsa-miR-199a-3p* were both considered (Fig. 5F), survival outcome of P subtype patients was changed. P subtype patients with lower than the median level of these two miRNAs had significantly longer survival time than those with a higher level than the median (Fig. 5F, p = 0.005).

hsa-miR-199a-3p inhibits cell viability and sensitizes U87S to TMZ

Furthermore, to explore the role of *hsa-miR-199a-3p* in gliomagenesis, we evaluated the endogenous expression level of *hsa-miR-199a-3p* in three cell lines, HA (astrocytes), U87MG (glioblastoma cells) and U87S (glioblastoma stem-like cells), and found that *hsa-miR-199a-3p* was expressed in all three cell lines, albeit at different levels. U87S cells had a significantly low level of *hsa-miR-199a-3p* expression compared to HA and U87MG (Fig. 6A, $p < 0.05$), indicating that *hsa-miR-199a-3p* expression is induced during differentiation. Next, we looked into the effect of *hsa-miR-199a-3p* on cell viability. Overexpression of *hsa-miR-199a-3p* in U87S cells caused a significant decrease of cell viability compared to the negative control (NC), both in TMZ- and TMZ + group (Fig. 6B, $p < 0.05$), indicating that *hsa-miR-199a-3p* can inhibit cell viability and enhance TMZ-mediated cytotoxicity.

Our previous results showed that BMP can sensitize U87S to TMZ, and up-regulate the expression of *hsa-miR-199a-3p*. Therefore we investigated whether BMP signaling affects the function of *hsa-miR-199a-3p* on cell viability. BMP2 (20 ng/ml) and LDN 193189 (200 nM) were utilized to activate and inhibit BMP signaling respectively as before. By checking cell viability, we observed that overexpression of *hsa-miR-199a-3p* with BMP2 treatment resulted in a significant decrease of cell viability compared with BMP2 treatment alone, and a mild but statistically significant decrease of cell viability compared with the one overexpressing *hsa-miR-199a-3p* without BMP activation (Fig. 6C, $p < 0.05$). Results indicated that BMP can boost *hsa-miR-199a-3p*-mediated cell viability inhibition in U87S cells. Next, we explored whether *hsa-miR-199a-3p* could affect BMP-mediated TMZ cytotoxicity in U87S cells. When U87S cells were exposed to 500 μM TMZ for 24 h s, co-treatment of BMP2 markedly reduced cell viability, and overexpression of *hsa-miR-199a-3p* mimics together with BMP2 treatment caused a further decrease of cell viability (Fig. 6D, $p < 0.05$). On the opposite, knockdown the endogenous *hsa-miR-199a-3p* together with BMP2 treatment partially increased cell viability (Fig. 6D, $p < 0.05$). Our results indicated that BMP and *hsa-miR-199a-3p* are working in an additive way to enhance TMZ-mediated cytotoxicity.

Putative targets of *hsa-miR-199a-3p* and clinic relevance

To better understand functions of *hsa-miR-199a-3p*, we predicted its targets and narrow down the target number to 1000 based on the differentially expressed mRNAs from our RNA sequencing data (unpublished). Among 1000 putative *hsa-miR-199a-3p* targets, GO analysis revealed that most target genes were enriched in the cellular process, metabolic process and biologic regulation (Fig. 7A). KEGG pathway analysis showed that the majority of *hsa-miR-199a-3p* targets were in the Rap1 signaling pathway (Fig. 7B). Next, we selected 5 putative targets of *hsa-miR-199a-3p* (AGAP3, TXNIP, SLC22A18, ANGPTL2 and CITED2), which were significantly down-regulated in BMP2 and BMP2-TMZ treated groups in our RNA-seq data (FPKM > 2, fold change ≥ 2, $P < 0.05$). qRT-PCR results showed expression patterns of these five genes were consistent with RNA-seq data, and in a negative correlation to *hsa-miR-199a-3p* (Fig. 7C), highly suggesting possible regulation between them. Furthermore, to explore the potential roles of these five genes in clinical, the expression patterns of these five genes in 156 TCGA GBM patients were queried (Fig. 7D). The results showed that AGAP3 was significantly down-regulated in GBM tumors (Fig. 7E, $p < 0.05$), while TXNIP, SLC22A18, and ANGPTL2 were significantly up-regulated in GBM tumors (Fig. 7F—I, $p < 0.001$), and the expression of CITED2 showed no significant difference between tumor and normal samples (Fig. 7H). Furthermore, the expression level of SLC22A18, which was significantly highly expressed in GBM tumors ($p < 0.001$), was found connected to the survival outcome of GBM patients. GBM patients with a lower expression level of SLC22A18 showed significantly longer survival time than ones with a higher expression level of SLC22A18 (Fig. 7J).

Construction of a *hsa-miR-199a-3p* mediated ceRNA network

Competitive endogenous RNAs (ceRNAs) have been known to play a role in posttranscriptional regulation in cancer cells, including GBM.[46] According to the ceRNA hypothesis, miRNAs are more likely to be a RNA bridge between non-coding RNAs and mRNAs. To systematically explore the influence of dynamic changes on gene expression by *hsa-miR-199a-3p* in glioblastoma stem-like cells, we constructed a *hsa-miR-199a-3p* mediated ceRNA network, integrating matched lncRNAs and mRNAs (Fig. 8). The *hsa-miR-199a-3p* mediated ceRNA network contained 189 mRNAs and 269 lnRNAs, which share common *hsa-miR-199a-3p* binding element, therefore can work as ceRNAs competing binding to *hsa-miR-199a-3p*. 5 putative targets of *hsa-miR-199a-3p* (AGAP3, TXNIP, SLC22A18, ANGPTL2 and CITED2) validated by qRT-PCR were marked in the network by blue circles. Based on the ceRNA network, long non-coding RNAs, NONHSAT152229.1 and NONHSAT149718.1 might compete with TXNIP for binding *hsa-miR-199a-3p*. NONHSAT212882.1 and NONHSAT253787.1 might compete with AGAP3 for binding *hsa-miR-199a-3p*. NONHSAT229594.1 likely competes with SLC22A18, and NONHSAT252752.1 likely competes with CITED2 for binding *hsa-miR-199a-3p*. Together, *hsa-miR-199a-3p* mediated ceRNA network shows a complicated post-transcriptional regulation for *hsa-miR-199a-3p*.

Discussion

Glioblastoma multiform (GBM), WHO grade IV, is the most lethal tumor of the central nervous system in adults with poor prognosis.[1,3] Glioblastoma stem-like cells (GSCs) in GBM are recognized for tumor-progression, treatment-resistant, and tumor recurrence.[6—8] Therefore, a promising therapy for GBM is to target GSCs. Bone morphogenetic proteins (BMPs) are known to be strong inducers of astroglial differentiation in GSC cells both *in vitro* and *in vivo*,[19,20] and BMPs can also render GSCs more susceptible to TMZ treatment.[17,21] So, BMP-mediated differentiation therapy has been proposed as a promising strategy for GBM therapy. However, GSCs have evolved mechanisms to evade BMP induced differentiation.[22] The study on the

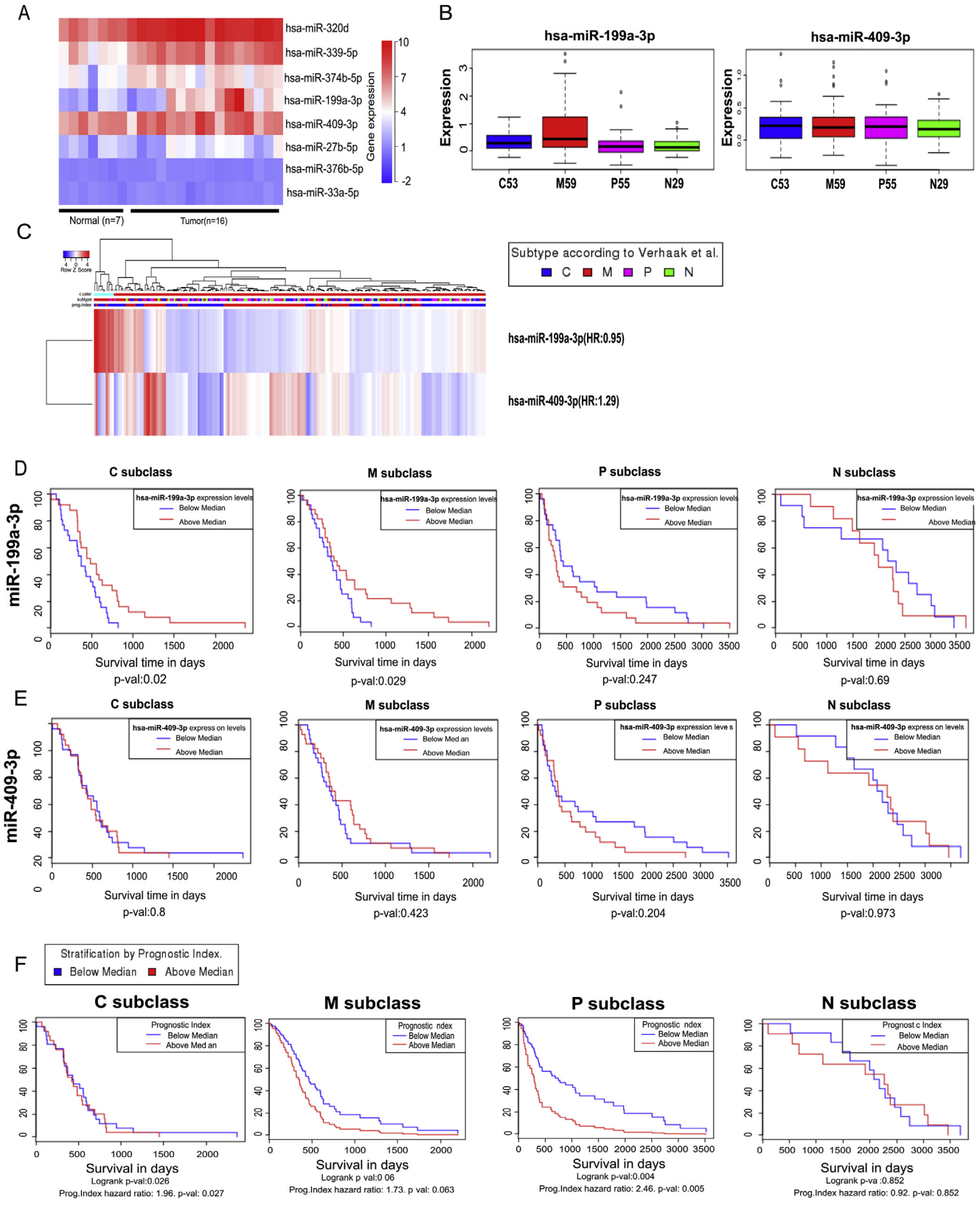

Figure 5 Clinic relevance of 8 validated miRNAs. **(A)** Heatmap of 8 validated miRNAs expression patterns in 7 normal brain tissues and 16 GBM patient tissues from GEO data. The color from blue to red represents the gene count number. *has-miR-320d*, *has-miR-339-5p*, *has-374b-5p* and *has-miR-199a-3p* were up-regulated in GBM tumors (fold change ≥ 2, $p < 0.05$). **(B)** Boxplot of the *hsa-199a-3p*and *has-miR-409-3p* expression distribution in four subtypes of GBM of 196 TCGA patients. *hsa-miR-199a-3p* shows significantly elevated expression in M subtype of GBM patients ($p = 0.001$). *has-miR-409-3p* does not show a significant difference among

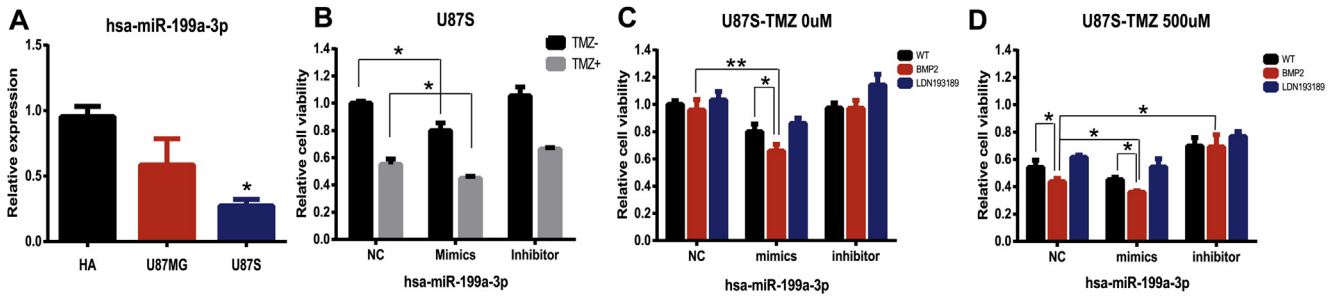

Figure 6 *hsa-miR-199a-3p* inhibits the proliferation and enhances TMZ chemosensitivity in U87S cells. **(A)** Detection of endogenous *hsa-miR-199a-3p* levels in HA, U87 MG, and U87S cells by RT-PCR. Data are presented as mean ± SD from three independent experiments. $*p < 0.05$ compared with HA. **(B)** The effect of *hsa-miR-199a-3p* on the proliferation and TMZ chemosensitivity in U87S. Cell viability was measured by CCK-8 assay in the U87S cells transfected with the *hsa-miR-199a-3p* mimics, *hsa-miR-199a-3p* inhibitor, or their corresponding negative control (miR-NC and anti-NC) with or without TMZ treatment respectively. Data are presented as mean ± SD from three independent experiments. $*p < 0.05$ compared to the NC group. (**C**) BMP activation boosts the inhibitory effect of *hsa-miR-199a-3p* on cell proliferation. Cell viability was measured by CCK-8 assay in the U87S cells transfected with the *hsa-miR-199a-3p* mimics, *hsa-miR-199a-3p* inhibitor or their corresponding negative control (miR-NC and anti-NC) with the endogenous BMP signaling (WT, black bars), activation of BMP signaling (BMP2, red bars), and inhibition of BMP signaling (LDN 193189, blue bars) respectively. Data are presented as mean ± SD from three independent experiments. $**p < 0.001$, $*p < 0.05$ compared to NC group. (**D**) *hsa-miR-199a-3p* and BMP sensitize TMZ chemosensitivity in an additive way. The U87S cells were transfected with the *hsa-miR-199a-3p* mimics, *hsa-miR-199a-3p* inhibitor or their corresponding negative control (miR-NC and anti-NC) with the endogenous BMP signaling (WT, black bars), activation of BMP signaling (BMP2, red bars), and inhibition of BMP signaling (LDN 193189, blue bars) respectively. 500 μM TMZ was used to treat cells for 24 h. Cell viability was measured with CCK-8 assay. Data are presented as mean ± SD from three independent experiments. $*p < 0.05$ compared to NC group.

underlying intracellular molecular mechanisms in GSCs is needed to improve outcomes towards BMP induced differentiation therapy.

In this study, we aim to identify the miRNA signatures associated with BMP and TMZ in glioblastoma stem-like cells. For it, we built a GSC cell model called U87S and examined its stem-cell traits and TMZ chemosensitivity. Our results proved that U87S is an ideal cell model for screening miRNAs related to BMP and TMZ. By RNA sequencing, we identified BMP-mediated and TMZ-mediated DE miRNAs. Bioinformatics analysis revealed that these DE miRNAs have important roles in gliomagenesis. One of the enriched pathways is the PI3K-Akt pathway. The PI3K-Akt pathway is one of the most important intracellular pathways, which is frequently aberrantly activated in diverse cancers, including GBM. It is a well-known fact that PI3K-Akt pathway plays a pivotal role in tumorigenesis and resistance of chemoradiotherapy in GBM.[47,48] The PI3K-Akt pathway can be activated by transmembrane tyrosine kinase growth factor receptors, such as EGFR (epidermal growth factor receptor), which is a well-known diagnostic and prognostic marker for GBM.[49] EGFR signaling has been reported to function in the acquisition of GSC characteristics and angiogenesis by induction of ID3 (inhibitor of differentiation 3) and ID3-regulated cytokines through AKT-dependent activation of Smad5.[50] So, the DE miRNAs identified in our study may not only function with BMP and TMZ, but also mediate the crosstalk of BMP signaling with other signal pathways in GSCs to regulate the progression of glioblastoma. Future study on the specific mechanism will be one of our interests.

One BMP-regulated miRNA, *hsa-miR-199a-3p*, from our screening, was differentially expressed in the mesenchymal (M) subtype of GBM. And its expression level was associated with survival outcome of patients. Further study showed that it was differentially expressed in U87S cells, and could inhibit cell viability and enhance TMZ-induced cell death, indicating its crucial role in gliomagenesis. The functions of *hsa-miR-199a-3p* in other cancers have also been reported.[51–54] *hsa-miR-199a-3p* showed the ability to inhibit cell proliferation in several cancer cells, including hepatocellular carcinoma, breast cancer, esophageal cancer, and prostate cancer, suggesting it's pivotal roles in regulating cell proliferation. Qu, F et al have reported that *hsa-miR-199a-3p* inhibited cell proliferation by targeting Smad1, an intracellular signal transducer of BMP, in prostate cancer cells.[52] In our study, we found that the activation of BMP signaling boosted the effect of *hsa-miR-199a-*

subtypes of GBM. (**C**) Heatmap of *hsa-miR-199a-3p* and *hsa-miR-409-3p* expression in four subtypes of GBM patients. *hsa-miR-199a-3p* and *hsa-miR-409-3p* have distinct expression patterns in GBM subtypes. (**D**) The relevance of *has-miR199a-3p* expression to the survival time of GBM patients in four subtypes by Kaplan-Meier analysis. Higher expression of *hsa-miR-199a-3p* in C subtype ($p = 0.02$) and M subtype ($p = 0.029$) is associated with better survival outcome. (**E**) The relevance of *hsa-miR-409-3p* expression to the survival time of GBM patients in four subtypes by Kaplan-Meier analysis. The expression level of *hsa-miR-409-3p* in each GBM subtype is not significantly associated with the survival time of patients. (**F**) Survival analysis with expressions of *hsa-199a-3p* and *hsa-miR-409-3p* both considered. P subtype patients with lower than the median level of *hsa-miR-199a-3p* and *hsa-miR-409-3p* have a longer survival time than those with the upper level than the median ($p = 0.005$).

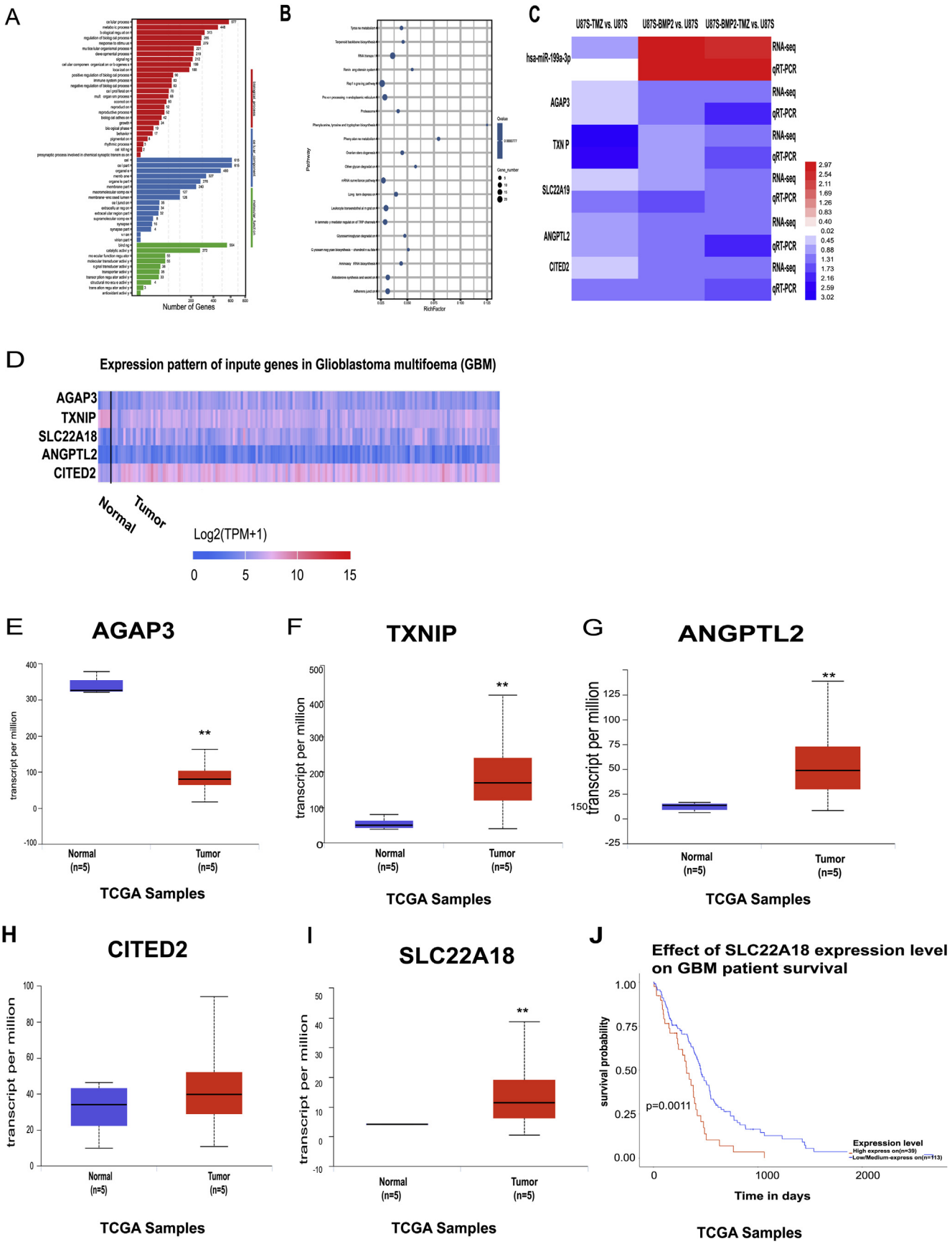

Figure 7 Putative targets of *hsa-miR-199a-3p*. (**A**) Functional enrichment analysis of putative 1000 target genes of *hsa-199a-3p* by GO. The bar chart represents the classification of GO Biological Processes, Cellular Component or Molecular Function. Bars

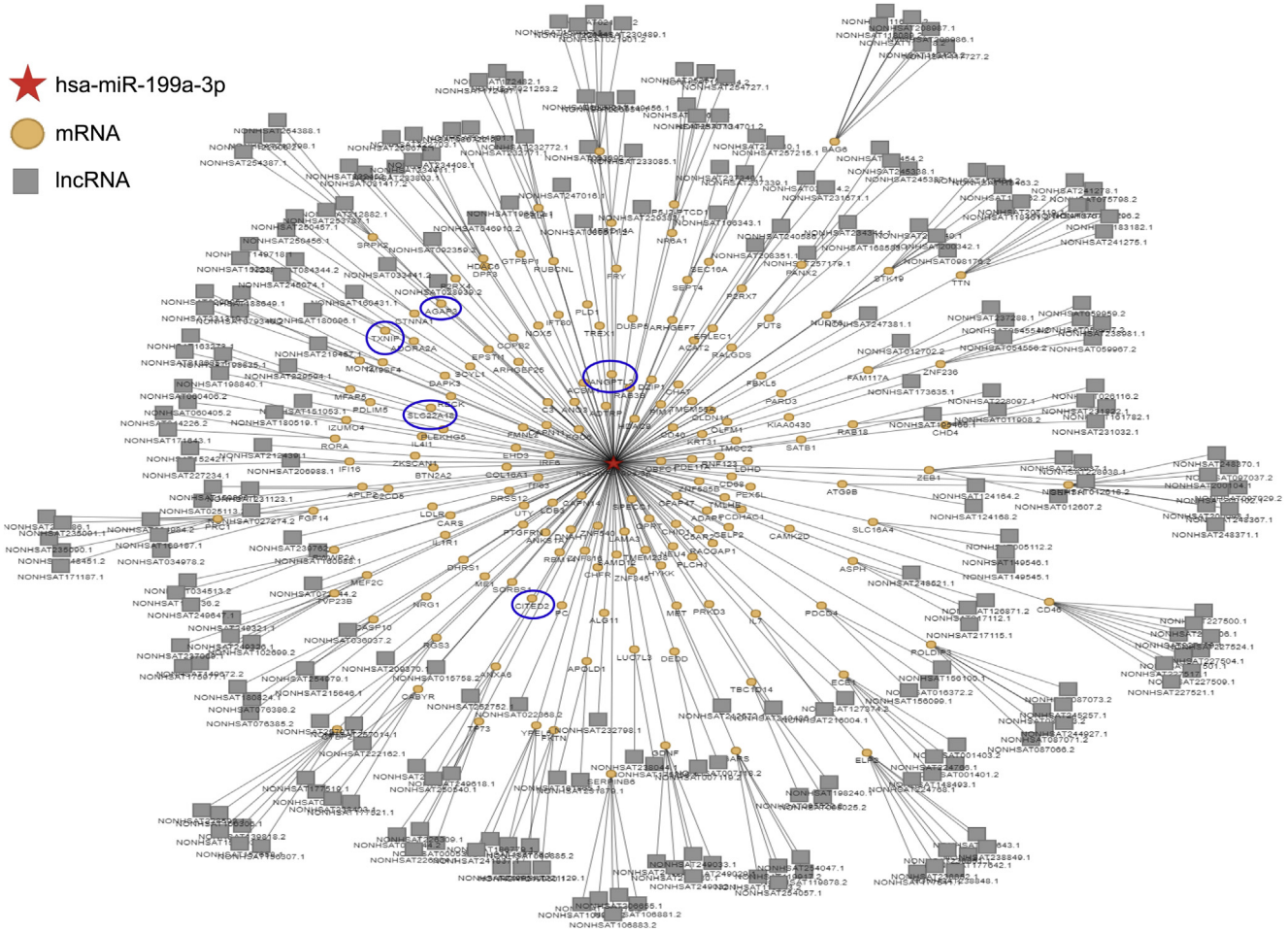

Figure 8 The *hsa-199a-3p*-mediated ceRNA network. The *hsa-miR-199a-3p* mediated ceRNA network contained 189 mRNAs and 269 lnRNAs, which share common *hsa-miR-199a-3p* binding elements, can work as ceRNAs competing binding to *hsa-miR-199a-3p*. 5 putative targets of *hsa-miR-199a-3p* (AGAP3, TXNIP, SLC22A18, ANGPTL2 and CITED2) validated by qRT-PCR were marked by blue circles.

3p on cell viability and TMZ-induced cell death. Further to find out whether BMP and *hsa-miR-199a-3p* function in a loop in GSC cells will be interesting.

GO and KEGG analysis with putative targets of *hsa-miR-199a-3p* revealed that they were primarily enriched in biological regulation and Rap1 pathway. Rap1, a Ras family GTPase, has been implicated in cancer cell proliferation and tumor cell growth.[55] The knockdown of Rap1A in the Rap1 signaling pathway in U373MG glioblastoma cells caused inhibition of cell proliferation.[55] Together with our finding, it is a reasonable guess that *hsa-miR-199a-3p*, up-regulated by BMP signaling in GSCs, might cause down-regulation of its targets in the Rap1 signaling pathway, therefore to inhibit cell proliferation of GSCs. The future study will be done to explore it.

In our study, we have analyzed five putative targets of *hsa-miR-199a-3p* (AGAP3, TXNIP, SLC22A18, ANGPTL2 and CITED2). Functional studied with them have been reported by others. CITED2, highly expressed in GBM by TCGA data, has been reported involved in the differentiation of GSCs.[56]

represent the number of genes in the specified category, organized by p-value. (**B**) The top 20 enriched signaling pathways for putative target genes of *hsa-199a-3p* by KEGG. Enriched pathways are selected based on the enrichment factor value with the number of genes in a pathway $\geq$4. The blue color from dark to light represents the Q value. The size of the dots represents the gene number in each pathway. (**C**) Heatmap shows expression patterns of has-miR-199a-3p and 5 of its predictive targets in RNA-seq and qRT-PCR (fold change $>$ 2 in the treated group compared to untreated U87S, $p < 0.005$). A negative correlation of *hsa-miR-199a-3p* and these five putative targets are shown both in RNA-seq and qRT-PCR data. Data are presented as mean $\pm$ SD ($n = 3$). Red color represents up-regulated and blue color represents down-regulated. (**D**) Heatmap of expressions of AGAP3, TXNIP, SLC22A18, ANGPTL2 and CITED2 in 156 TCGA GBM patient samples compared to normal brain tissue. (**E**) Boxplot of the expression pattern of AGAP3. (**F**) Boxplot of the expression pattern of TXNIP. (**G**) Boxplot of the expression pattern of ANGPTL2. (**H**) Boxplot of the expression pattern of CITED2. (**I**) Boxplot of the expression pattern of SLC22A18. (**J**) Kaplan-Meier plot shows the association of SLC22A18 expression with patient survival. Lower expression of SLC22A18 than medium leads to longer survival time for patients.

SLC22A18, highly expressed in GBM, is related to the chemosensitivity of glioma cells.[57] ANGPTL2, up-regulated in GBM, is associated with the proliferation and invasion of glioma cells. The knockdown of ANGPTL2 caused an inhibitory effect of cell proliferation and invasion on glioma cells.[58] Further study of how these genes precipitate in the process of BMP2-mediated TMZ chemosensitivity in GSCs will be worth doing.

Furthermore, in this study, we constructed *hsa-miR-199a-3p*-mediated ceRNA network (miRNA-mRNA-lncRNA). The network showed that the mRNA and lncRNA can work as ceRNAs competing binding to *hsa-miR-199a-3p*. When the time for functional study of *hsa-miR-199a-3p* involved in BMP-mediated TMZ chemosensitvity, a complicated post-transcriptional regulatory network should be taken in consideration.

Altogether, our results identified the miRNA signature regulated by BMPs and associated with TMZ in GSCs. Our findings may shed light to better understand intracellular mechanisms of BMP mediated TMZ chemosensitivity in GSCs, and may lead to finding out miRNA-based target therapies that specially target GSCs and improve outcomes towards BMP induced differentiation therapy for GBM.

Conflicts of interest

No competing financial interests exist.

Acknowledgements

We would like to thank Dr. Richard W. Padgett from University of Rutgers, U.S.A. for his meaningful advice on this study. This work was partially supported by grants from the National Natural Science Foundation of China (31501039), Chongqing Yuzhong District Science and technology project (20140104), Chongqing Basic and Frontier Research Project (cstc2016jcyjA0305), Open Project of Key Laboratory of Oncology and Immunology of Ministry of Education (2012jszl10) to YL, and the National Natural Science Foundation of China (81473284) to LW.

Appendix A. Supplementary data

Supplementary data to this article can be found online at https://doi.org/10.1016/j.gendis.2019.09.002.

References

1. Luo JW, Wang X, Yang Y, Mao Q. Role of micro-RNA (miRNA) in pathogenesis of glioblastoma. *Eur Rev Med Pharmacol Sci*. 2015;19(9):1630—1639.
2. Wick W, Osswald M, Wick A, Winkler F. Treatment of glioblastoma in adults. *Ther Adv Neurol Disord*. 2018;11, 1756286418790452.
3. Delgado-Lopez PD, Corrales-Garcia EM. Survival in glioblastoma: a review on the impact of treatment modalities. *Clin Transl Oncol*. 2016;18(11):1062—1071.
4. Filatova A, Acker T, Garvalov BK. The cancer stem cell niche(s): the crosstalk between glioma stem cells and their microenvironment. *Biochim Biophys Acta*. 2013;1830(2):2496—2508.
5. Qiang L, Yang Y, Ma YJ, et al. Isolation and characterization of cancer stem like cells in human glioblastoma cell lines. *Cancer Lett*. 2009;279(1):13—21.
6. Sundar SJ, Hsieh JK, Manjila S, Lathia JD, Sloan A. The role of cancer stem cells in glioblastoma. *Neurosurg Focus*. 2014;37(6):E6.
7. Rycaj K, Tang DG. Cancer stem cells and radioresistance. *Int J Radiat Biol*. 2014;90(8):615—621.
8. Bao S, Wu Q, McLendon RE, et al. Glioma stem cells promote radioresistance by preferential activation of the DNA damage response. *Nature*. 2006;444(7120):756—760.
9. Gomez-Puerto MC, Iyengar PV, Garcia de Vinuesa A, Ten Dijke P, Sanchez-Duffhues G. Bone morphogenetic protein receptor signal transduction in human disease. *J Pathol*. 2019;247(1):9—20.
10. Lissenberg-Thunnissen SN, de Gorter DJ, Sier CF, Schipper IB. Use and efficacy of bone morphogenetic proteins in fracture healing. *Int Orthop*. 2011;35(9):1271—1280.
11. Sanchez-Duffhues G, Hiepen C, Knaus P, Ten Dijke P. Bone morphogenetic protein signaling in bone homeostasis. *Bone*. 2015;80:43—59.
12. Hegarty SV, O'Keeffe GW, Sullivan AM. BMP-Smad 1/5/8 signalling in the development of the nervous system. *Prog Neurobiol*. 2013;109:28—41.
13. Katagiri T, Watabe T. Bone morphogenetic proteins. *Cold Spring Harb Perspect Biol*. 2016;8(6).
14. Caja L, Bellomo C, Moustakas A. Transforming growth factor beta and bone morphogenetic protein actions in brain tumors. *FEBS Lett*. 2015;589(14):1588—1597.
15. Yamada N, Kato M, ten Dijke P, et al. Bone morphogenetic protein type IB receptor is progressively expressed in malignant glioma tumours. *Br J Cancer*. 1996;73(5):624—629.
16. Liu C, Tian G, Tu Y, Fu J, Lan C, Wu N. Expression pattern and clinical prognostic relevance of bone morphogenetic protein-2 in human gliomas. *Jpn J Clin Oncol*. 2009;39(10):625—631.
17. Gonzalez-Gomez P, Anselmo NP, Mira H. BMPs as therapeutic targets and biomarkers in astrocytic glioma. *Biomed Res Int*. 2014;2014:549742.
18. Xi G, Best B, Mania-Farnell B, James CD, Tomita T. Therapeutic potential for bone morphogenetic protein 4 in human malignant glioma. *Neoplasia*. 2017;19(4):261—270.
19. Rampazzo E, Dettin M, Maule F, et al. A synthetic BMP-2 mimicking peptide induces glioblastoma stem cell differentiation. *Biochim Biophys Acta Gen Subj*. 2017;1861(9):2282—2292.
20. Piccirillo SG, Reynolds BA, Zanetti N, et al. Bone morphogenetic proteins inhibit the tumorigenic potential of human brain tumour-initiating cells. *Nature*. 2006;444(7120):761—765.
21. Persano L, Pistollato F, Rampazzo E, et al. BMP2 sensitizes glioblastoma stem-like cells to Temozolomide by affecting HIF-1alpha stability and MGMT expression. *Cell Death Dis*. 2012;3:e412.
22. Yan K, Wu Q, Yan DH, et al. Glioma cancer stem cells secrete Gremlin1 to promote their maintenance within the tumor hierarchy. *Genes Dev*. 2014;28(10):1085—1100.
23. Bartel DP. MicroRNAs: genomics, biogenesis, mechanism, and function. *Cell*. 2004;116(2):281—297.
24. Lewis BP, Burge CB, Bartel DP. Conserved seed pairing, often flanked by adenosines, indicates that thousands of human genes are microRNA targets. *Cell*. 2005;120(1):15—20.
25. Ahir BK, Ozer H, Engelhard HH, Lakka SS. MicroRNAs in glioblastoma pathogenesis and therapy: a comprehensive review. *Crit Rev Oncol Hematol*. 2017;120:22—33.
26. Masoudi MS, Mehrabian E, Mirzaei H. MiR-21: a key player in glioblastoma pathogenesis. *J Cell Biochem*. 2018;119(2):1285—1290.

27. Visani M, de Biase D, Marucci G, et al. Expression of 19 microRNAs in glioblastoma and comparison with other brain neoplasia of grades I—III. *Mol Oncol*. 2014;8(2):417—430.
28. Munthe S, Halle B, Boldt HB, et al. Shift of microRNA profile upon glioma cell migration using patient-derived spheroids and serum-free conditions. *J Neurooncol*. 2017;132(1):45—54.
29. Liu S, Yin F, Zhang J, et al. Regulatory roles of miRNA in the human neural stem cell transformation to glioma stem cells. *J Cell Biochem*. 2014;115(8):1368—1380.
30. Wang Z, Gerstein M, Snyder M. RNA-Seq: a revolutionary tool for transcriptomics. *Nat Rev Genet*. 2009;10(1):57—63.
31. Mortazavi A, Williams BA, McCue K, Schaeffer L, Wold B. Mapping and quantifying mammalian transcriptomes by RNA-Seq. *Nat Methods*. 2008;5(7):621—628.
32. t Hoen PA, Ariyurek Y, Thygesen HH, et al. Deep sequencing-based expression analysis shows major advances in robustness, resolution and inter-lab portability over five microarray platforms. *Nucleic Acids Res*. 2008;36(21):e141.
33. Yang YH, Dudoit S, Luu P, et al. Normalization for cDNA microarray data: a robust composite method addressing single and multiple slide systematic variation. *Nucleic Acids Res*. 2002;30(4):e15.
34. Kruger J, Rehmsmeier M. RNAhybrid: microRNA target prediction easy, fast and flexible. *Nucleic Acids Res*. 2006;34(Web Server issue):W451—W454.
35. John B, Enright AJ, Aravin A, Tuschl T, Sander C, Marks DS. Human MicroRNA targets. *PLoS Biol*. 2004;2(11):e363.
36. Agarwal V, Bell GW, Nam JW, Bartel DP. Predicting effective microRNA target sites in mammalian mRNAs. *Elife*. 2015;4.
37. Celiku O, Johnson S, Zhao S, Camphausen K, Shankavaram U. Visualizing molecular profiles of glioblastoma with GBM-BioDP. *PLoS One*. 2014;9(7), e101239.
38. Chandrashekar DS, Bashel B, Balasubramanya SAH, et al. UALCAN: a portal for facilitating tumor subgroup gene expression and survival analyses. *Neoplasia*. 2017;19(8):649—658.
39. Kanehisa M, Araki M, Goto S, et al. KEGG for linking genomes to life and the environment. *Nucleic Acids Res*. 2008;36(Database issue):D480—D484.
40. Shervington A, Lu C. Expression of multidrug resistance genes in normal and cancer stem cells. *Cancer Invest*. 2008;26(5):535—542.
41. Liu G, Yuan X, Zeng Z, et al. Analysis of gene expression and chemoresistance of CD133+ cancer stem cells in glioblastoma. *Mol Cancer*. 2006;5:67.
42. Yokoyama Y, Watanabe T, Tamura Y, Hashizume Y, Miyazono K, Ehata S. Autocrine BMP-4 signaling is a therapeutic target in colorectal cancer. *Cancer Res*. 2017;77(15):4026—4038.
43. Verhaak RG, Hoadley KA, Purdom E, et al. Integrated genomic analysis identifies clinically relevant subtypes of glioblastoma characterized by abnormalities in PDGFRA, IDH1, EGFR, and NF1. *Cancer Cell*. 2010;17(1):98—110.
44. Zhang W, Zhang J, Hoadley K, et al. miR-181d: a predictive glioblastoma biomarker that downregulates MGMT expression. *Neuro Oncol*. 2012;14(6):712—719.
45. Kouri FM, Ritner C, Stegh AH. miRNA-182 and the regulation of the glioblastoma phenotype - toward miRNA-based precision therapeutics. *Cell Cycle*. 2015;14(24):3794—3800.
46. Yuan Y, Jiaoming L, Xiang W, et al. Analyzing the interactions of mRNAs, miRNAs, lncRNAs and circRNAs to predict competing endogenous RNA networks in glioblastoma. *J Neurooncol*. 2018;137(3):493—502.
47. Li X, Wu C, Chen N, et al. PI3K/Akt/mTOR signaling pathway and targeted therapy for glioblastoma. *Oncotarget*. 2016;7(22):33440—33450.
48. Polivka Jr J, Janku F. Molecular targets for cancer therapy in the PI3K/AKT/mTOR pathway. *Pharmacol Ther*. 2014;142(2):164—175.
49. Mazzoleni S, Politi LS, Pala M, et al. Epidermal growth factor receptor expression identifies functionally and molecularly distinct tumor-initiating cells in human glioblastoma multiforme and is required for gliomagenesis. *Cancer Res*. 2010;70(19):7500—7513.
50. Jin X, Yin J, Kim SH, et al. EGFR-AKT-Smad signaling promotes formation of glioma stem-like cells and tumor angiogenesis by ID3-driven cytokine induction. *Cancer Res*. 2011;71(22):7125—7134.
51. Ren K, Li T, Zhang W, Ren J, Li Z, Wu G. miR-199a-3p inhibits cell proliferation and induces apoptosis by targeting YAP1, suppressing Jagged1-Notch signaling in human hepatocellular carcinoma. *J Biomed Sci*. 2016;23(1):79.
52. Qu F, Zheng J, Gan W, et al. MiR-199a-3p suppresses proliferation and invasion of prostate cancer cells by targeting Smad1. *Oncotarget*. 2017;8(32):52465—52473.
53. Phatak P, Burrows WM, Chesnick IE, et al. MiR-199a-3p decreases esophageal cancer cell proliferation by targeting p21 activated kinase 4. *Oncotarget*. 2018;9(47):28391—28407.
54. Fan X, Zhou S, Zheng M, Deng X, Yi Y, Huang T. MiR-199a-3p enhances breast cancer cell sensitivity to cisplatin by down-regulating TFAM (TFAM). *Biomed Pharmacother — Biomed Pharmacother*. 2017;88:507—514.
55. Sayyah J, Bartakova A, Nogal N, Quilliam LA, Stupack DG, Brown JH. The Ras-related protein, Rap1A, mediates thrombin-stimulated, integrin-dependent glioblastoma cell proliferation and tumor growth. *J Biol Chem*. 2014;289(25):17689—17698.
56. Kolosa K, Motaln H, Herold-Mende C, Korsic M, Lah TT. Paracrine effects of mesenchymal stem cells induce senescence and differentiation of glioblastoma stem-like cells. *Cell Transplant*. 2015;24(4):631—644.
57. Chu SH, Ma YB, Feng DF, Li ZQ, Jiang PC. Predictive value of the SLC22A18 protein expression in glioblastoma patients receiving temozolomide therapy. *J Transl Med*. 2013;11:69.
58. Yang LK, Zhu J, Chen YH, et al. Knockdown of angiopoietin-like protein 2 inhibits proliferation and invasion in glioma cells via suppressing the ERK/MAPK signaling pathway. *Oncol Res*. 2017;25(8):1349—1355.